ORGANOMETALLICS
Article

Organometallics **2010,** *29,* 1717–1728 1717
DOI: 10.1021/om9011104

Controlling Selectivity in Intermolecular Alkene or Aldehyde Hydroacylation Reactions Catalyzed by $\{Rh(L_2)\}^+$ Fragments

Rebekah J. Pawley,[†] Gemma L. Moxham,[‡] Romaeo Dallanegra,[†] Adrian B. Chaplin,[†] Simon K. Brayshaw,[‡] Andrew S. Weller,*[,†,‡] and Michael C. Willis[†,‡]

[†]*Department of Chemistry, Inorganic Chemistry Laboratory, University of Oxford, South Parks Road, Oxford, OX1 3QR, U.K., and* [‡]*Department of Chemistry, University of Bath, Bath, BA2 7AY, U.K.*

Received December 23, 2009

Rhodium(III) dihydrido complexes $[Rh(L_2)(H)_2(acetone)][BAr^F{}_4]$ ($Ar^F = C_6H_3(CF_3)_2$) containing the potentially hemilabile ligands L_2 = 9,9-dimethyl-4,5-bis(diphenylphosphino)xanthene (Xantphos) and $[Ph_2P(CH_2)_2]_2O$ (POP′) have been prepared from their corresponding norbornadiene rhodium(I) precursors. In solution these complexes are fluxional by proposed acetone dissociation, which can be trapped out by addition of MeCN to form $[Rh(L_2)(H)_2(NCMe)][BAr^F{}_4]$, which have been crystallographically characterized. Addition of alkene (methyl acrylate) to these complexes results in reduction to a rhodium(I) species and when followed by addition of the aldehyde $HCOCH_2CH_2SMe$ affords the new acyl hydrido complexes $[Rh(L_2)(COCH_2CH_2SMe)H][BAr^F{}_4]$ in good yield. The solid-state and solution structures show a tight binding of the POP′ and Xantphos ligands, having a *trans*-arrangement of the phosphines with the central ether linkage bound. This is similar to the previously reported complex [Rh(DPEphos)-$(COCH_2CH_2SMe)H][BAr^F{}_4]$ (DPEphos = $[Ph_2P(C_6H_4)]_2O$). Unlike the DPEphos complex, the Xantphos and POP′ ligated complexes are not effective catalysts for the hydroacylation reaction between methyl acrylate and $HCOCH_2CH_2SMe$. This is traced to their inability to dissociate the central ether link in a hemilabile manner to reveal a vacant site necessary for alkene coordination. Consistent with this lack of availability of the vacant site, these complexes also are stable toward reductive decarbonylation. Complexes $[Rh(Ph_2P(CH_2)_nPPh_2)(acetone)_2][BAr^F{}_4]$ (n = 2−5) have also been studied as catalysts for the hydroacylation reaction between methyl acrylate and $HCOCH_2CH_2SMe$ at 22 °C. As found previously, for n = 2 this affords the product of alkene hydroacylation, but as the chain length is progressively increased to n = 5, the reaction also progressively changes to favor the product of aldehyde hydroacylation. This is suggested to occur by a decrease in the accessibility of the metal site on increasing the bite angle of the chelate ligand, so that alkene coordination to a putative Rh(III)-acyl hydrido intermediate is progressively disfavored and aldehyde coordination (followed by hydride transfer) is progressively favored. These, and previous, results show that the overall conversion in the hydroacylation reaction can be controlled by the hemilabile nature of the chelating phosphine in the catalyst (e.g., DPEphos versus Xantphos), and the course of the reaction can also be tuned by changing the bite angle of the phosphine, cf. $Ph_2P(CH_2)_2PPh_2$ and $Ph_2P(CH_2)_5PPh_2$.

Introduction

The transition-metal-catalyzed hydroacylation reaction that couples alkenes, or alkynes, with aldehydes is an attractive atom-efficient method for the formation of unsymmetrical ketones, eq 1.[1,2] It has attracted significant attention in recent years, and a variety of—mainly rhodium-based—catalyst systems have been developed.[3−15] Similar carbonyl hydroacylation systems have also been described.[16−19] The key steps in

*Corresponding author. E-mail: andrew.weller@chem.ox.ac.uk.

(1) Suggs, J. W. *J. Am. Chem. Soc.* **1978**, *100*, 640–641.
(2) Willis, M. C. *Chem. Rev.* **2009**, *110*, 725−748.
(3) Fairlie, D. P.; Bosnich, B. *Organometallics* **1988**, *7*, 946–954.
(4) Fairlie, D. P.; Bosnich, B. *Organometallics* **1988**, *7*, 936–945.
(5) Marder, T. B.; Roe, D. C.; Milstein, D. *Organometallics* **1988**, *7*, 1451–1453.
(6) Kundu, K.; McCullagh, J. V.; Morehead, A. T., Jr. *J. Am. Chem. Soc.* **2005**, *127*, 16042–16043.
(7) Jun, C. H.; Jo, E. A.; Park, J. W. *Eur. J. Org. Chem.* **2007**, 1869–1881.
(8) Roy, A. H.; Lenges, C. P.; Brookhart, M. *J. Am. Chem. Soc.* **2007**, *129*, 2082–2093.
(9) Lenges, C. P.; White, P. S.; Brookhart, M. *J. Am. Chem. Soc.* **1998**, *120*, 6965–6979.
(10) Shibata, Y.; Tanaka, K. *J. Am. Chem. Soc.* **2009**, *131*, 12552–12553.
(11) Coulter, M. M.; Dornan, P. K.; Dong, V. M. *J. Am. Chem. Soc.* **2009**, *131*, 6932–6933.
(12) Osborne, J. D.; Randell-Sly, H. E.; Currie, G. S.; Cowley, A. R.; Willis, M. C. *J. Am. Chem. Soc.* **2008**, *130*, 17232–17233.
(13) Osborne, J. D.; Willis, M. C. *Chem. Commun.* **2008**, 5025–5027.
(14) Willis, M. C.; Randell-Sly, H. E.; Woodward, R. L.; McNally, S. J.; Currie, G. S. *J. Org. Chem.* **2006**, *71*, 5291–5297.
(15) Willis, M. C.; McNally, S. J.; Beswick, P. J. *Angew. Chem., Int. Ed.* **2004**, *43*, 340–343.
(16) Bergens, S. H.; Fairlie, D. P.; Bosnich, B. *Organometallics* **2002**, *9*, 566–571.
(17) Fuji, K.; Morimoto, T.; Tsutsumi, K.; Kakiuchi, K. *Chem. Commun.* **2005**, 3295–3297.
(18) Phan, D. H. T.; Kim, B.; Dong, V. M. *J. Am. Chem. Soc.* **2009**, *131*, 15608–15609.
(19) Shen, Z.; Dornan, P. K.; Khan, H. A.; Woo, T. K.; Dong, V. M. *J. Am. Chem. Soc.* **2009**, *131*, 1077–1091.

© 2010 American Chemical Society
Published on Web 03/01/2010

Scheme 1. Hemilabile DPEphos, Protecting the Vacant Site[a]

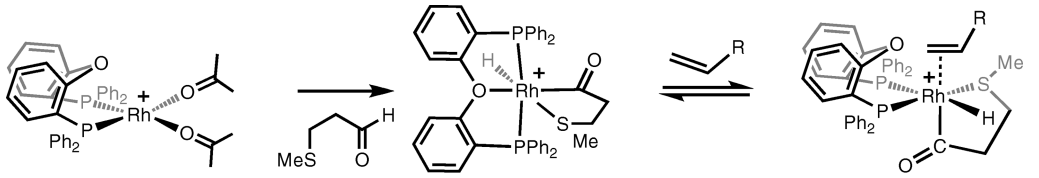

1a

[a] Anions are omitted for clarity.

the mechanism have been identified and involve oxidative addition of aldehyde to a Rh(I) center to give a hydrido-acyl species, followed by migratory insertion of an η-bound alkene (or heteroalkene), and reductive elimination of the C−C coupled product.[3,19−22] A major obstacle in the development of this potentially powerful disconnection in organic synthetic methodology is competing reductive decarbonylation, which results in an inactive metal carbonyl. This occurs from a low-coordinate intermediate in the catalytic cycle, which can undergo migratory deinsertion of a carbonyl from an acyl group to a *cis* vacant site, followed by reductive elimination of a saturated product (e.g., R-H).

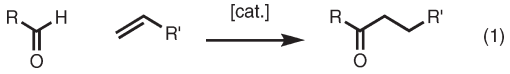

(1)

Various strategies have been adopted to attenuate this detrimental decarbonylation pathway, one being chelation control from the substrate.[1,7,15,23] We have recently reported an alternative metal−ligand-based approach to this problem by using the hemilabile[24] phosphine-ether ligand DPEphos [bis(2-diphenylphosphinophenyl) ether[25]] to protect the vacant site, thus stabilizing the catalyst toward decarbonylation, while also being able to move away to allow approach of substrate (e.g., Scheme 1).[21,26] This produces an efficient intermolecular catalyst that can couple β-S-substituted aldehydes and unactivated alkenes such as 1-octene.

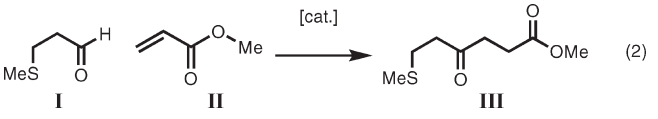

I **II** **III** (2)

In this contribution we build upon these results by describing the effect that changing the hemilabile ligand has on the rate and selectivity of the hydroacylation reaction between the β-S-substituted aldehyde, $HCOCH_2CH_2SMe$ **I**, and methyl acrylate **II** to afford the coupled product **III** (eq 2). We find that when using the ligands Xantphos (9,9-dimethyl-4,5-bis-(diphenylphosphino)xanthene)[25] or (POP′) ($[Ph_2P(CH_2)_2]_2O$),

Chart 1. The Bidentate Ligands Used in This Study

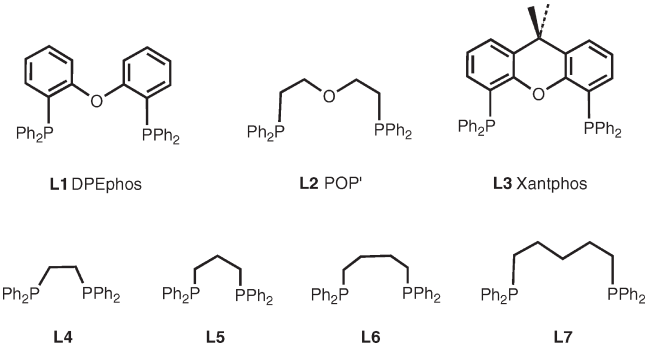

catalytic reactivity is significantly attenuated, while for the chelating, but nonhemilabile ligands $Ph_2P(CH_2)_nPPh_2$ (n = 2−5, Chart 1) the unexpected result of switching the reaction from almost exclusively alkene hydroacylation (n = 2) to almost exclusively aldehyde hydroacylation (Tishchenko-type[27] product, n = 5) is revealed. One of us has recently reported a related switch in reactivity between hydroacylation and reductive aldol on moving between DPEphos and dppe ligands in rhodium-based catalyst systems.[13]

Results

A study of the hydroacylation reaction using rhodium catalysts requires a suitable Rh(I) precursor entry point. A library of these are readily generated by the synthesis of the corresponding cationic norbornadiene adducts partnered with the weakly coordinating anion $[BAr^F{}_4]^-$ (Ar^F = C_6H_3-$(CF_3)_2$). Chart 1 shows the phosphines used, and Scheme 2 summarizes the complexes made. These are all isolated as crystalline materials in good yield. Complexes **2** and **4**−**7** have previously been reported as different salts.[4,28] Care has to be taken in the synthesis of [Rh(**L4**)(nbd)][$BAr^F{}_4$] (**4**, nbd = norbornadiene) to avoid the contaminant [Rh(**L4**)$_2$]-[$BAr^F{}_4$], and a revised procedure allows for this (Experimental Section). $^{31}P\{^1H\}$ NMR, ^1H NMR, and ESI-MS spectra of these norbornadiene complexes are in full accord with their formulation as Rh(I) pseudo-square-planar complexes. Notably single ^{31}P environments showing coupling to ^{103}Rh consistent with the Rh(I) center [e.g., **3** δ 9.74, J(RhP) 142 Hz] are observed for all species. Active precatalysts can be accessed via addition of H_2 to these norbornadiene adducts in acetone solution.[29] We discuss first those complexes formed with the POP′ (**L2**) and Xantphos (**L3**) ligands.

(20) Benhamou, L.; Cesar, V.; Lugan, N.; Lavigne, G. *Organometallics* **2007**, *26*, 4673–4676.
(21) Moxham, G. L.; Randell-Sly, H.; Brayshaw, S. K.; Weller, A. S.; Willis, M. C. *Chem.—Eur. J.* **2008**, *14*, 8383–8397.
(22) Hyatt, I. F. D.; Anderson, H. K.; Morehead, A. T.; Sargent, A. L. *Organometallics* **2008**, *27*, 135–147.
(23) Tanaka, K.; Shibata, Y.; Suda, T.; Hagiwara, Y.; Hirano, M. *Org. Lett.* **2007**, *9*, 1215–1218.
(24) Braunstein, P.; Naud, F. *Angew. Chem., Int. Ed.* **2001**, *40*, 680–699.
(25) Kranenburg, M.; Vanderburgt, Y. E. M.; Kamer, P. C. J.; Vanleeuwen, P.; Goubitz, K.; Fraanje, J. *Organometallics* **1995**, *14*, 3081–3089.
(26) Moxham, G. L.; Randell-Sly, H. E.; Brayshaw, S. K.; Woodward, R. L.; Weller, A. S.; Willis, M. C. *Angew. Chem., Int. Ed.* **2006**, *45*, 7618–7622.
(27) Crimmin, M. R.; Barrett, A. G. M.; Hill, M. S.; Procopiou, P. A. *Org. Lett.* **2007**, *9*, 331–333.
(28) Brown, J. M.; Chaloner, P. A.; Kent, A. G.; Murrer, B. A.; Nicholson, P. N.; Parker, D.; Sidebottom, P. J. *J. Organomet. Chem.* **1981**, *216*, 263–276.
(29) Schrock, R. R.; Osborn, J. A. *J. Am. Chem. Soc.* **1976**, *98*, 2134–2143.

Scheme 2. Synthesis of the Rh(I) Norbornadiene Precursors

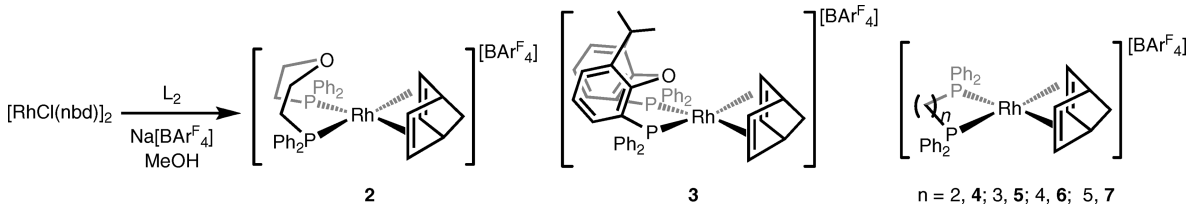

Scheme 3. Sequential Reaction of 2 with H_2 (8), Alkene (10), and Aldehyde (11) or MeCN (9)[a]

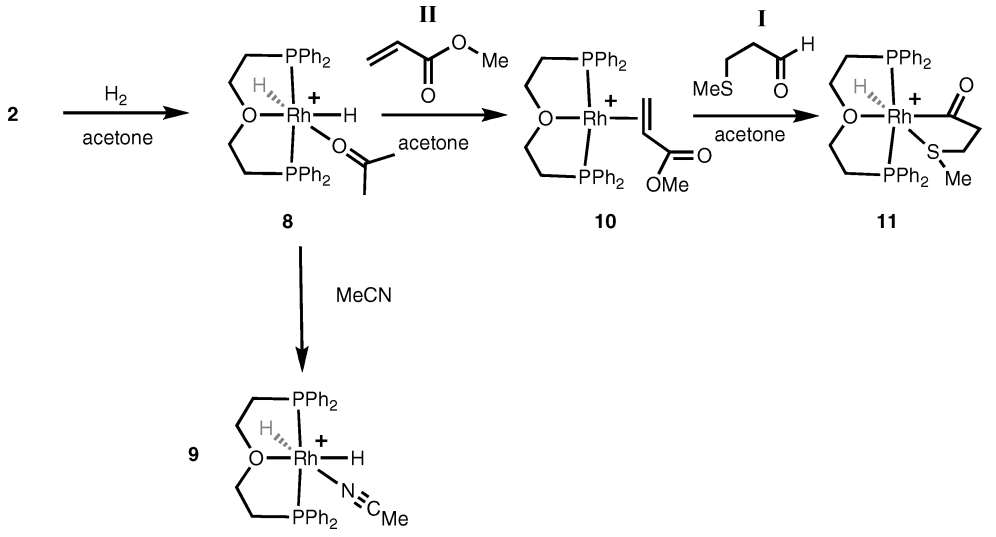

[a] $[BAr^F_4]^-$ anions are not shown.

Addition of H_2 (1−4 atm) to an acetone solution of **2** results in the hydrogenation of the strained norbornadiene ligand and the formation of the Rh(III) hydrido complex $[Rh(\mathbf{L2})(H)_2(acetone)][BAr^F_4]$ (**8**) (Scheme 3), which was characterized by NMR spectroscopy and ESI-MS. The room-temperature ^1H NMR spectrum of **8** shows a broad, relative integral 2H, peak at δ −19.84 assigned to the hydride ligands; while there is a single ^{31}P environment (δ 48.4) showing coupling to ^{103}Rh [J(RhP) 121 Hz] in the $^{31}P\{^1H\}$ NMR spectrum. On cooling (225 K), the hydride peak splits into two multiplets in a 1:1 ratio, indicating inequivalent hydride environments, viz., δ −19.25 and −20.27. The coupling in these signals is best described as an overlapping doublet of triplets of doublets and has been simulated successfully and also probed using $^1H\{^{31}P\}$ decoupling experiments, in which the hydride signals collapse into two doublets of doublets, demonstrating coupling to two equivalent ^{31}P nuclei. The size of the coupling to the phosphines and the other hydride places them all mutually *cis* [J(PH) ∼14, J(HH) 11 Hz]. The $^{31}P\{^1H\}$ NMR spectrum at this temperature shows one phosphorus environment, δ 49.0, showing coupling to ^{103}Rh [121 Hz]. These data suggest a likely structure for **8** that has a *trans*-spanning POP′ ligand,[30] *cis* hydrides, and the sixth coordination site occupied by acetone. The low-temperature data discount a five-coordinate pseudo-trigonal-bipyramidal structure with equivalent hydride ligands. It also argues against a five-coordinate square-based pyramid with a vacant site *trans* to the hydride, as the hydride resonances do not show distinctive high-field shifts associated with hydride ligands *trans* to a vacant site.[31] These chemical shifts are similar to those reported for related six-coordinate pincer systems, such as [(PCP-^{i}Pr)Rh(H)(acetone)$_2$][BF_4], δ −21.29 [PCP-^{i}Pr = 1,3-bis(di-isopropylphosphinomethyl)benzene].[32] We also discount an alternative structure for **8** that invokes *trans*-hydrides (with the POP′ ligand either *cis* or *trans* spanning), as such species might be expected to show chemical shifts for the hydrides that are much less shielded,[33] e.g., *trans*-[(PNP)Ir(CO)(H)$_2$][PF_6] (δ −6.63)[34] and *trans*-[^{i}Pr-PONOP)Ru(H)$_2$(PPh_3] (δ −6.09)[35] [PNP = 2,6-bis-(di-*tert*-butylphosphinomethyl)pyridine, ^{i}Pr-PONOP = C_5H_3-N-1,3-(OP^{i}Pr$_2$)$_2$]. The observed fluxionality at room temperature is likely due to a mechanism that passes through a five-coordinate intermediate, via loss of acetone, that makes the hydride ligands equivalent on the NMR time scale. ESI-MS (electrospray ionization mass spectrometry) shows a peak at m/z = 605.1 (calcd 605.1), which corresponds to the suggested formulation, and a major peak at m/z = 547.1 identified as $[M]^+$ − acetone (calcd 547.1). The methanol adduct analogous to **8**, [Rh(**L2**)(H)$_2$(MeOH)][BF_4], has been reported by Brown[36] and has very similar spectroscopic characteristics. The isolation of a

(30) Bessel, C. A.; Aggarwal, P.; Marschilok, A. C.; Takeuchi, K. *J. Chem. Rev.* **2001**, *101*, 1031–1066.

(31) Cooper, A. C.; Clot, E.; Huffman, J. C.; Streib, W. E.; Maseras, F.; Eisenstein, O.; Caulton, K. G. *J. Am. Chem. Soc.* **1999**, *121*, 97–106.

(32) Montag, M.; Schwartsburd, L.; Cohen, R.; Leitus, G.; Ben-David, Y.; Martin, J. M. L.; Milstein, D. *Angew. Chem., Int. Ed.* **2007**, *46*, 1901–1904.

(33) Grellier, M.; Vendier, L.; Sabo-Etienne, S. *Angew. Chem., Int. Ed.* **2007**, *46*, 2613−2615, and references therein.

(34) Kloek, S. M.; Heinekey, D. M.; Goldberg, K. I. *Organometallics* **2006**, *25*, 3007–3011.

(35) Salem, H.; Shimon, L. J. W.; Diskin-Posner, Y.; Leitus, G.; Ben-David, Y.; Milstein, D. *Organometallics* **2009**, *28*, 4791–4806.

(36) Brown, J. M.; Cook, S. J.; Kent, A. G. *Tetrahedron* **1986**, *42*, 5097–5104.

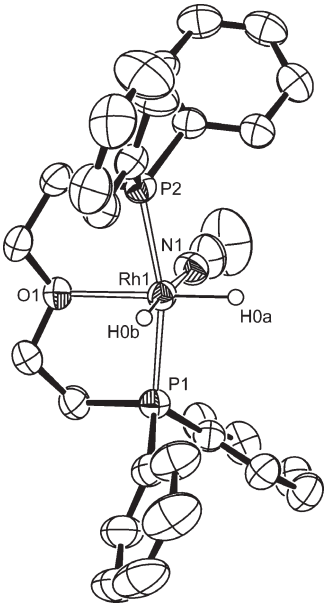

Figure 1. Molecular structure of the cationic portion of [Rh(**L2**)$(H)_2$(NCMe)][BAr^F_4], **9**. Ellipsoids are drawn at the 50% probability level. The anion and hydrogen atoms, apart from H0A and H0B, are omitted for clarity. Selected bond lengths (Å): Rh1−P1, 2.2765(10); Rh1−P2, 2.2778(10); Rh1−O1, 2.232(3); Rh1−N1, 2.134(4). Selected bond angles (deg): P1−Rh1−P2, 164.95(4); N1−Rh1−O1, 89.97(12).

Rh(III) dihydride species is in contrast to the Rh(I) bis-acetone adduct that is formed with the DPEphos ligand.[21] Addition of MeCN to acetone solutions of **8** afforded the acetonitrile adduct [Rh(**L2**)$(H)_2$(NCMe)][BAr^F_4], **9**, which was characterized by NMR spectroscopy and ESI-MS. ^{1}H and ^{31}P{^{1}H} NMR spectra for **9** are very similar to those of **8** observed at 225 K, showing that the fluxional process observed in **8** is acetone dissociation: the more strongly bound MeCN in **9** is reluctant to dissociate. The solid-state structure of **9** has also been established by X-ray crystallography, Figure 1, and this shows it to have a meridinal POP′ ligand, *cis* hydrides, and a coordinated MeCN ligand, as suggested by the NMR data for the solution structure of the acetone adduct **8**.

A suitable Rh(I) precursor that can enter the catalytic cycle comes from adding excess methyl acrylate, **II**, to an acetone solution of **8**. This results in the transfer of the hydrides to the unsaturated substrate, coordination of another equivalent of alkene, and the generation *in situ* of a complex spectroscopically characterized by ^{1}H and ^{31}P{^{1}H} NMR spectroscopy and ESI-MS as the Rh(I) alkene adduct [Rh(**L2**)(η^2-H_2C=$CHCO_2$Me)][BAr^F_4], **10**. The ^{31}P{^{1}H} NMR spectrum shows a doublet at δ 39.1 [J(RhP) 129 Hz], while in the ^{1}H NMR spectrum broad signals attributable to bound olefin are observed at δ 3.60−2.64, which are similar to those reported for (triphos)Rh(H)(η^2-H_2C=$CHCO_2$Me).[37] Excess methyl acrylate is observed as broadened signals (δ 6.41−5.82 and 3.70), this suggesting an exchange between both bound and free alkene, although we have not attempted to determine a rate constant for this. ESI-MS shows a parent ion at m/z = 631.1 (calcd 631.1), confirming the empirical formula. MS/MS interrogation of this peak forces the loss of methyl acrylate, giving an ion at m/z = 545.1 (calcd 545.1), further supporting the suggested formulation.

(37) Bianchini, C.; Meli, A.; Peruzzini, M.; Vizza, F.; Bachechi, F. *Organometallics* **1991**, *10*, 820–823.

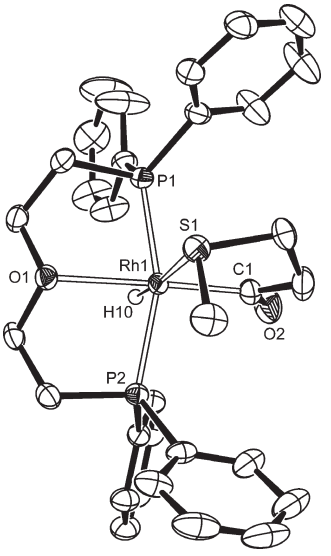

Figure 2. Molecular structure of the cationic portion of [Rh(**L2**)($COCH_2CH_2SMe$)H][BAr^F_4], **11**. The anion and hydrogen atoms, apart from H10, are omitted for clarity. Ellipsoids are drawn at the 50% probability level. Selected bond lengths (Å): Rh1−H10, 1.51(2); Rh1−C1, 1.969(2); Rh1−P2, 2.2938(4); Rh1−P1, 2.2971(5); Rh1−O1, 2.302(1); Rh1−S1, 2.4369(4). Selected bond angles (deg): P2−Rh1−P1, 156.21(2); C1−Rh1−S1, 87.57(6); H10−Rh1−S1, 174.5(9); C1−Rh1−O1, 177.17(6). C1−S1−Rh1−O1 torsion, 88.4(2)°.

Chart 2

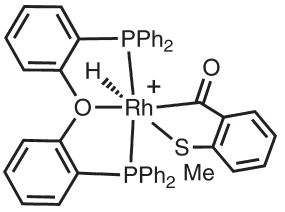

1b

Addition of aldehyde **I** to an acetone solution of **10**, generated *in situ*, affords the product of aldehyde oxidative addition, [Rh(**L2**)($COCH_2CH_2SMe$)H][BAr^F_4], **11**, in essentially quantitative yield by NMR spectroscopy. The solid-state structure of **11** is shown in Figure 2, which shows a Rh(III) species with a *trans*-spanning POP′ ligand and the hydride and thioether ligands mutually *trans*-orientated. It is very closely related to that of **1b**, [Rh(DPEphos)(COC_6H_4SMe)H][$CB_{11}H_6Cl_6$] (Chart 2).[21] The phosphorus atoms sit approximately *trans* to one another [P1−Rh1−P1 156.21(2)°], similar to **1b** [155.93(5)°]. The Rh−O distance in **11** is longer than that in **1b** [2.3017(12) versus 2.248(3) Å, respectively], although, as noted later, the ether ligand in **11** is not displaced by incoming ligands (e.g., MeCN), unlike **1a/b**, which readily form the corresponding MeCN adducts. The reasons for this difference in reactivity are not clear, given the trend in the bond lengths, but they might reflect the difference in backbone ligand architecture between POP′ and DPEphos. The SMe group is canted to one side, making the two phosphorus atoms chemically inequivalent. This is as observed for **1b** in the solid state and for **1a** (Scheme 1) from low-temperature solution NMR data.

The room-temperature ^{31}P{^{1}H} NMR spectrum of **11** shows a broad signal at δ 31.1. A single hydride environment

Scheme 4. Addition of H_2 to 3[a]

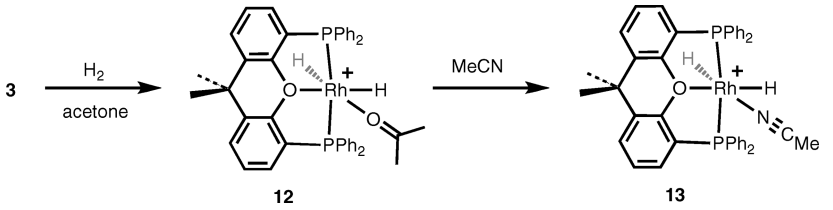

[a] $[BAr^F_4]^-$ anions are not shown.

at δ −9.58 is observed as a broadened doublet [J(RhH) 24 Hz], while the $^1H-^1H$ COSY NMR spectrum shows a correlation between the hydride and the SMe group (δ 1.79); the latter appears as a doublet. The single resonance in the $^{31}P\{^1H\}$ NMR spectrum splits into a tightly coupled ABX spectrum on cooling to 225 K, with two resonances observed at δ 34.6 and 28.5 that show *trans* $^{31}P-^{31}P$ coupling, J(PP) 309 Hz, as well as coupling to ^{103}Rh, consistent with a Rh(III) center, viz., 128, 133 Hz. We have previously observed similar fluxional behavior in solution for **1a** and **1b**, which was suggested to be due to an inversion of stereochemistry at the thioether, resulting in a flip of the methyl group from side to side via a sp^2-hybridized at sulfur intermediate.[21] The coupling between the methyl and hydride groups observed at room temperature shows that the Rh−S bond is not broken in this fluxional process.

Complex **11** is stable toward decarbonylation, remaining unchanged in d_6-acetone solution over a period of 1 week as monitored by NMR spectroscopy and ESI-MS. This is in contrast to **1a**, which reductively decarbonylates over the same time scale to give [Rh(**L1**)(CO)(EtSMe)][$CB_{11}H_6Cl_6$], while [Rh(**L4**)($COCH_2CH_2SMe_2$)(H)]$^+$ cannot be isolated, as decarbonylation is rapid.[21] The stability of **11** is no doubt related to the tight binding of the POP′ ligand, which does not decoordinate the ether linkage and thus does not reveal the *cis* vacant site necessary for migratory decarbonylation. This tight binding is further established by the fact that addition of excess MeCN (100 equiv) to an acetone solution of **11** does not displace the ether ligand, to the detection limits of a $^{31}P\{^1H\}$ NMR experiment. This is in contrast to **1a/b**, which immediately form the MeCN adducts, alongside concomitant decoordination of the hemilabile ether. Similarly, addition of methyl acrylate to **11** did not result in reaction, again in contrast to **1a/b**, which proceed to give the product of hydroacylation.[21]

Similar to the formation of **8**, hydrogenation of the Xantphos (**L3**) precursor **3** in acetone results in the formation of dihydrido species [Rh(**L3**)$(H)_2$(acetone)][BAr^F_4], **12** (Scheme 4). The NMR data for **12** are similar to **8**, and we thus assign a similar structure in which the ligand is proposed to be *trans*-spanning coordinating through the central oxygen with *cis* hydrides. A single ^{31}P environment is observed in the room-temperature $^{31}P\{^1H\}$ NMR spectrum, δ 45.4 [J(RhP) 121 Hz], while in the ^{1}H NMR spectrum two broad, relative integral 1 H, hydride environments, δ −18.81 and −19.00, are observed. One broad methyl signal is also observed for the Xantphos ligand. Cooling to 225 K resolves the hydride signals into two sharp multiplets at approximately the same chemical shift as at room temperature, which show mutually *cis* coupling to the other hydride and ^{31}P as well as coupling to ^{103}Rh [doublet of triplets of doublets]. The $^{31}P\{^1H\}$ NMR spectrum remains unchanged at this temperature. ESI-MS confirms the empirical formulation (m/z = 741.15, calcd 741.15). The observation of two, albeit broad, hydride environments at room temperature for **12**, in contrast to the one seen for **8**, suggests a larger barrier to the fluxional process that makes the hydrides equivalent for the latter. Similar to **8** addition of MeCN to acetone solutions of **12** results in the formation of an acetonitrile adduct, [Rh(**L3**)$(H)_2$(NCMe)][BAr^F_4] (**13**), and a sharpening of the hydride resonances, consistent with the cessation of the fluxional processes. **13** has been characterized by ^{1}H and ^{31}P NMR spectroscopy and ESI-MS and shows similar solution data to **9**. The solid-state structure of **13** has also been established by X-ray crystallography (Figure 3), and this shows it to have a *trans*-spanning[38−40] Xantphos ligand, *cis* hydrides, and a coordinated MeCN ligand. This geometry is also as suggested by NMR data for the solution structures of the acetone adducts **8** and **12**.

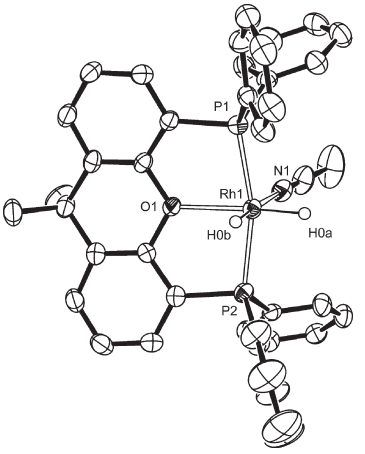

Figure 3. Molecular structure of the cationic portion of [Rh(**L3**)$(H)_2$(NCMe)][BAr^F_4], **13**. Ellipsoids are drawn at the 50% probability level. The anion and hydrogen atoms, apart from H0A and H0B, are omitted for clarity. Selected bond lengths (Å): Rh1−P1, 2.2748(8); Rh1−P2, 2.2584(8); Rh1−O1, 2.233(2); Rh1−N1, 2.128(3). Selected bond angles (deg): P1−Rh1−P2, 164.31(3); N1−Rh1−O1, 95.98(9).

Addition of excess methyl acrylate **II** to acetone solutions of **12** gave a material in solution that was tentatively characterized by ^{1}H NMR, $^{31}P\{^1H\}$ NMR, and ESI-MS as [Rh(**L3**)(η^2-H_2C=CHCOOMe)][BAr^F_4], **14**, by comparison with the solution analytical data for **10**. Addition of aldehyde **I** to acetone solutions of **14** formed in this way afforded the product of oxidative addition of aldehyde to a Rh(I) center,

(38) van der Veen, L. A.; Keeven, P. H.; Schoemaker, G. C.; Reek, J. N. H.; Kamer, P. C. J.; van Leeuwen, P. W. N. M.; Lutz, M.; Spek, A. L. *Organometallics* **2000**, *19*, 872–883.
(39) Sandee, A. J.; van der Veen, L. A.; Reek, J. N. H.; Kamer, P. C. J.; Lutz, M.; Spek, A. L.; van Leeuwen, P. *Angew. Chem., Int. Ed.* **1999**, *38*, 3231–3235.
(40) Zuideveld, M. A.; Swennenhuis, B. H. G.; Boele, M. D. K.; Guari, Y.; van Strijdonck, G. P. F.; Reek, J. N. H.; Kamer, P. C. J.; Goubitz, K.; Fraanje, J.; Lutz, M.; Spek, A. L.; van Leeuwen, P. *J. Chem. Soc., Dalton Trans.* **2002**, 2308–2317.

Scheme 5. Synthesis of Complex 15[a]

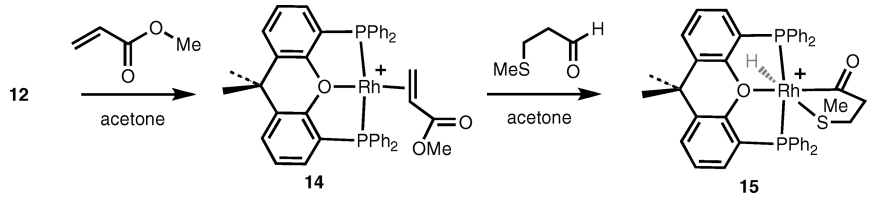

[a] $[BAr^F_4]^-$ anion is not shown.

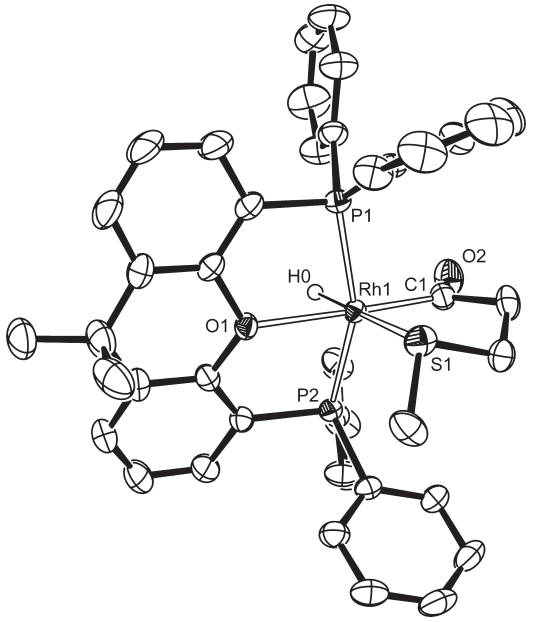

Figure 4. Molecular structure of the cationic portion of [Rh(**L3**)-$(COCH_2CH_2SMe)H][BAr^F_4]$, **15**. Major disordered component shown. The anion and hydrogen atoms, apart from H0, are omitted for clarity. Ellipsoids are drawn at the 50% probability level. Selected bond lengths (Å): Rh1−H0 1.58(2), Rh1−C1, 1.981(3); Rh1−P2, 2.2841(8); Rh1−P1, 2.2896(8); Rh1−O1, 2.308(2); Rh1−S1, 2.4431(9). Selected bond angles (deg): P2−Rh1−P1, 157.60(3); C1−Rh1−S1, 86.60(11); H0−Rh1−S1, 180(2); C1−Rh1−O1, 176.31(12). C4−S−Rh1−O1 torsion, 121.3(8)°.

$[Rh(\mathbf{L3})(COCH_2CH_2SMe)H][BAr^F_4]$, **15**, in essentially quantitative yield, which is directly comparable to **11** and **1a**/**b** (Scheme 5). The solid-state structure of **15** is shown in Figure 4, and this shows a *trans*-spanning Xantphos ligand coordinated to a Rh(III) acyl hydride. The thio-ether group is disordered over two sites, related by a small change in the twist of the S-Me group and a slight conformational change in the ethyl backbone. This was modeled successfully, and only the major component is shown. A related complex, Ir(**L3**)(CO)-$(H)_2(COEt)$, with a *cis*-coordinated Xantphos ligand has recently been reported.[41] The stereochemistry around the metal center in **15** is approximately the same as observed for **1b** and **11** in the solid state, the Rh−O distance being 2.308(2) Å and the P−Rh−P angle measured as 157.60(3)°. It is thus no surprise to find that the solution NMR data are very similar to these two complexes. In particular in the room-temperature ^1H NMR spectrum a broad doublet is observed at δ −8.72 [J(RhH) 23 Hz], the methylene protons of the aldehyde are observed as two, broad, integral 2 H signals at δ 2.62 and 2.04, and the Xantphos methyl groups are observed as two sharp, integral 3 H, singlets at δ 1.97 and 1.51. The S-Me group is observed at δ 1.47 as an unresolved, integral 3 H, multiplet that also shows a weak correlation to the hydride signal at δ −8.72 in a $^1H/^1H$ COSY experiment. The $^{31}P\{^1H\}$ NMR spectrum shows a broad signal at δ 32.8. These data indicate a fluxional process that makes equivalent the phosphorus atoms but not the Xantphos methyl groups. As for **11** and **1a**/**b**, a process that involves inversion at sulfur is most likely. Cooling to 257 K slows this process so that two sharp phosphorus environments are now observed in the $^{31}P\{^1H\}$ NMR spectrum that show an ABX coupling pattern with *trans* $^{31}P-^{31}P$ coupling [J(PP) 300 Hz]. At low temperature the hydride resonance is essentially unchanged although slightly better resolved than at room temperature. Four separate resonances for the methylene protons of the aldehyde backbone are also observed, consistent with a static structure. As found for **11**, complex **15** is stable toward decarbonylation over 1 week (by ESI-MS and NMR spectroscopy), while addition of MeCN does not displace the ether group, both observations demonstrating a tight binding of the *trans*-spanning ether ligand.

Complexes **11** and **15** do not react with methyl acrylate, **II**, remaining unchanged over 24 h on addition of a 10-fold-excess, as measured by NMR spectroscopy and ESI-MS. This is in direct contrast to **1a/b**, which react rapidly to give the product of hydroacylation.[21] This lack of reactivity is in line with the unavailability of the vacant site due to the strong binding of the ether linkage in the POP′ or Xantphos ligands. The norbornadiene precursor materials (**2** and **3**) were also screened in the catalysis of the hydroacylation reaction between aldehyde **I** and methyl acrylate **II**, after activation with H_2 (i.e., to form complexes **8** and **12**, respectively, *in situ*). As Table 1 shows (entries 2 and 3), these species are very poor catalysts for the hydroacylation reaction (product **III**), and over an extended time (∼150 h) the product of aldehyde hydroacylation, **IV** (formally a Tishchenko reaction[27,42]), is also formed, interestingly in a greater proportion than the alkene hydroacylation product. This overall low reactivity is consistent the attenuated-*hemilabile* nature of the phosphine ligands **L2** and **L3** and a resulting reactivity impasse at the acyl-hydride product.

Given that ligands **L2** and **L3** did not readily reveal a vacant site, we have explored the reactivity of a ligand that would do this but give similar electronic and steric profiles otherwise: $Ph_2P(CH_2)_5PPh_2$ (**L7**). As a further point of reference, we also prepared the complexes with the common bidentate phosphines $Ph_2P(CH_2)_nPPh_2$ (n = 2−4, **L4**−**L6**, Chart 1) and $[Rh(Ph_2P-(CH_2)_nPPh_2)(nbd)][BAr^F_4]$, **4**−**7** (Scheme 2). These complexes have been prepared previously as alternate salts.[4,28] Addition of H_2 (d_6-acetone solution) afforded the previously reported bis-acetone adducts $[Rh(Ph_2P(CH_2)_nPPh_2)(acetone)_2][BAr^F_4]$,

(41) Fox, D. J.; Duckett, S. B.; Flaschenriem, C.; Brennessel, W. W.; Schneider, J.; Gunay, A.; Eisenberg, R. *Inorg. Chem.* **2006**, *45*, 7197–7209.

(42) Seki, T.; Nakajo, T.; Onaka, M. *Chem. Lett.* **2006**, *35*, 824–829.

Table 1. Comparison of the Catalysts Reported in This Study in the Hydroacylation Reaction of I and II[a]

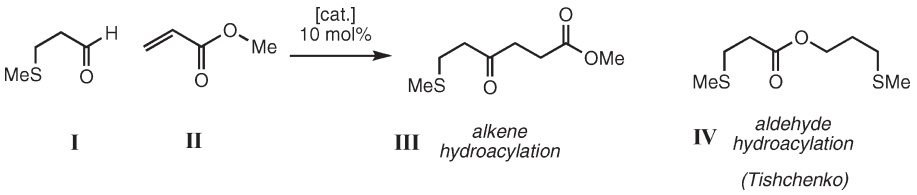

entry	ligand	temp (°C)	% alkene hydroacylation **III**	% aldehyde hydroacylation **IV**	total conversion of aldehyde	time (h)	initial rate for the formation of **III** $\times 10^{-3}$ (mol/L/h)[c]	initial rate for the formation of **IV** $\times 10^{-3}$ (mol/L/h)[c]
1	**L1**	22	93	7	100	20	96(6)	3(1)
2	**L2**	22	6	44	50[d]	165	10(7)	38(12)
3	**L3**	22	10	20	30[d]	145	2(2)	2.0(4)
4	**L4**	22	91	8	99[d]	60	30(2)	1.0(3)
5	**L5**	22	38	62	100	100	21(1)	25.0(3)
6	**L6**	22	50	50	100	8	134(10)	136(9)
7	**L7**	22	13	87	100	6	14(7)	130(2)
8	**L7**	40	17	83	100	0.5	[e]	[e]
9	**L7**	55	19	81	100	0.1	[e]	[e]
10[b]	**L7**	18	30	46	76	15	76(8)	140(20)

[a] Conditions: all manipulations under an argon atmosphere, 0.043 M solution of precatalyst in d_6-acetone, hydrogenated using standard procedures, catalyst:aldehyde ratio = 1:10, substrate ratio = 1:1 aldehyde:alkene, conversion determined by ^{1}H NMR spectroscopy. [b] Substrate ratio 1:5 aldehyde: alkene. [c] Initial rate determined from an exponential fit to the data at $t = 0$. [d] Total conversion at given time. [e] Reaction almost complete before a reliable first data point can be taken to determine an initial rate.

Scheme 6. Synthesis of Complexes 14 to 17[a]

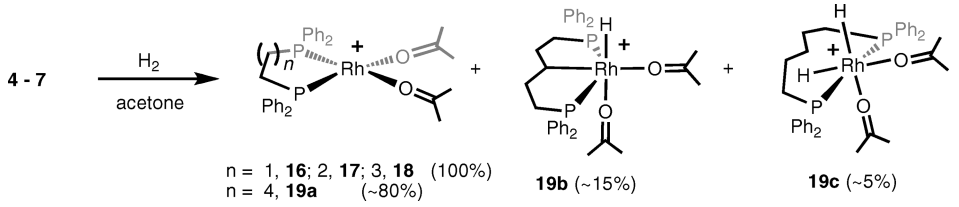

[a] $[BAr^F_4]^-$ anions are not shown.

16−**19**,[4] Scheme 6. Surprisingly, to our knowledge, the adduct with $Ph_2P(CH_2)_5PPh_2$ has not been reported, and we find it exists as a mixture of the Rh(I) bis-acetone complex [Rh(**L7**)(acetone)$_2$][BAr^F_4] (**19a**) and two Rh(III) hydrido species, which are tentatively characterized as the C−H activated complex [Rh(PPh$_2$CH$_2$CH$_2$CHCH$_2$CH$_2$PPh$_2$)(H)(acetone)$_2$][BAr^F_4] (**19b**) and the dihydride acetone adduct [Rh(**L7**)(H)$_2$(acetone)$_2$][BAr^F_4] (**19c**) (Scheme 6). Complex **19b** shows a hydride resonance in the ^{1}H NMR spectrum at δ −21.68 [J(PH) 16, J(RhH) 27 Hz] as a doublet of triplets that collapses into a doublet on decoupling ^{31}P, while **19c** shows a doublet of triplets at δ −22.30 [J(PH) 11, J(RhH) 35 Hz] that collapses into broad doublet on decoupling ^{31}P. The relative integral of these signals compared to the aromatic region (32 H) is 0.20 H (**19b**) and 0.14 H (**19c**). Three environments are also observed in the ^{31}P{^{1}H} NMR spectrum, δ 37.3 [d, J(RhP) 201], 35.8 [d, J(RhP) 115 Hz], and 55.3 [d, J(RhP) 133 Hz] in a 10:2:0.8 ratio (**19a**, **19b**, and **19c**, respectively, as determined by ^{1}H{^{31}P-selective} experiments). ESI-MS shows a signal due to the [Rh(**L7**)(acetone)$_2$][BAr^F_4] (m/z = 659.2, calcd 659.2) fragment. **19a** and **19b** have the same empirical formula (m/z 659.2), while the signals for the minor component **19c** would be masked by the isotope pattern for **19a/b**. Cooling a d_6-acetone solution of this mixture results in no significant change in chemical shifts, although the ratios do change slightly in favor of **19b**, perhaps suggesting a slow equilibrium between the three. Similar complexes to **19** have been reported previously as the methanol adducts and show very similar spectroscopic data.[28] These complexes are also in equilibrium with one another. The observation of dihydrido species on hydrogenation of rhodium(I) chelating phosphines with increasing bite angle of the phosphine (cf. **L4** and **L7**) has also been noted previously.[43,44]

Addition of aldehyde **I** to **16**−**19** did not afford species that were readily characterized, with multiple species observed by ^{31}P{^{1}H} NMR spectroscopy that turned into uncharacterized decomposition products over time. This is as previously reported by Bosnich for some of these systems with 4-pentenals.[3] However for **19** (**L7**) ESI-MS showed a relatively clean spectrum with a strong signal corresponding to the molecular ion [Rh(**L7**)(HCOCH$_2$CH$_2$SMe)$_2$]$^+$ (m/z = 751.15, calcd 751.15). Efforts to isolate this species lead to intractable material. These observations are in contrast to **1**, **11**, and **15** and reflect the controlling influence of ligands **L1**, **L2**, and **L3**, respectively, on both the stereochemical rigidity and overall stability of the Rh(III) acyl hydride complexes. Importantly, under these conditions **19b/c** were not observed by ESI-MS or NMR

(43) DuBois, D. L.; Blake, D. M.; Miedaner, A.; Curtis, C. J.; DuBois, M. R.; Franz, J. A.; Linehan, J. C. *Organometallics* **2006**, *25*, 4414−4419, and references therein.
(44) James, B. R.; Mahajan, D. *Can. J. Chem.: Rev. Can. Chim.* **1980**, *58*, 996–1004.

spectroscopy, suggesting that they react with aldehyde to give the same product as **19a**. This would be consistent with an equilibrium between the three, as suggested.

Complexes **16** to **19** (generated *in situ* by addition of H_2 to the nbd precursors) were screened as catalysts in the hydroacylation reaction between aldehyde **I** and methyl acrylate **II** at 10 mol % loading. Willis and co-workers have successfully used $\{Rh(\mathbf{L4})\}^+$, generated *in situ*, at higher temperature (60 °C) with aldehyde **I** and methyl acrylate **II** in intermolecular hydroacylation,[15,21,45] building upon Bosnich's early report of its use in the intramolecular hydroacylation of 4-pentenal.[4] Fu has reported on $\{Rh(\mathbf{L4})\}^+$ in the intramolecular hydroacylation of alkynes.[46] Ligand **L5** has also been used by a number of research groups in intramolecular hydroacylation reactions that invoke $\{Rh(\mathbf{L5})\}^+$ fragments as active catalysts.[19,23]

Table 1 lists the results of this catalyst screening and also compares these results with those from use of ligands **L1**, **L2**, and **L3**. Ligand **L4** under these conditions promotes complete conversion of the aldehyde over 60 h, but, interestingly, an approximate ratio of 9:1 of alkene hydroacylation, **III**, to aldehyde hydroacylation, **IV**, is observed by ^{1}H NMR spectroscopy (entry 4). Ligand **L4** has previously been reported to be effective for selective alkene hydroacylation at 55 °C over 2 h using these substrates, and the longer times for complete conversion under these conditions reported here are consistent with the lower temperature.[26] These higher temperatures also favor the formation of **III**. Repeating the reaction at 55 °C resulted in a shorter reaction time (2 h) and complete conversion to **III**. These conditions reported previously also use an excess of alkene, which would be expected to promote alkene hydroacylation. Unexpectedly, use of ligand **L7** results in a switch in product distribution, giving the *aldehyde* hydroacylation product **IV** as the major product in 87% conversion (entry 7). Heating to 40 and 55 °C using the catalyst derived from **L7** results in a gradual increase in alkene hydroacylation product **III** (entries 8 and 9), while use of a 5-fold excess of alkene also results in an increase in the yield of the alkene hydroacylation product (entry 10), although the rate of catalysis drops. Bosnich has previously reported substrate inhibition in intermolecular alkene hydoacylation,[3] which in our case presumably arises from competition for a vacant site prior to oxidative addition of the aldehyde. When using ligands **L5** and **L6**, products **III** and **IV** are observed in more equal proportions (entries 5 and 6). These data show that gradually increasing the length of the ligand backbone results in the products of aldehyde hydroacylation being favored. Figure 5 shows time/conversion plots of alkene versus aldehyde hydroacylation for these systems. For the systems and conditions reported here ligand **L1** performs the best in terms of selectivity and rate for alkene hydroacylation. This mirrors our previously reported results for this system at higher temperature (55 °C).[21]

Why does the reactivity change as the ligand backbone length (**L4** to **L7**) is changed? As noted, ligands **L2** and **L3** (entries 2 and 3) in complexes **11** and **15** do not move aside on approach of a relatively strong ligand such as acetonitrile or methyl acrylate, and thus the modest reactivity with alkene **II** is perhaps no surprise. It is also well established that chelate ring size, and in particular the bite angle, of the ligand can affect the rate of reaction and selectivity in many catalytic processes. Efforts to put these influences of the ligand on a quantitative footing have led to a number of closely related concepts. A large *natural bite angle* of a ligand can lead to enhanced rates of reductive elimination or selectivity, as exemplified in hydroformylation or hydrocyanation reations.[25,38,47−49] Barron and co-workers introduced the concept of *pocket angle*,[50] which relates the interior cone angle of a ligand (as influenced by the bite angle) to relative catalytic activity, with an optimum size of the pocket angle determined by a balance of accessibility of the metal center by the substrate with catalyst decomposition. The concept of *accessible molecular surface* (AMS), as developed by Leitner and co-workers,[51] provides a further refinement on the steric control of a chelating phosphine on catalysis in $\{Rh(L_2)\}^+$ fragments (L = chelating phosphine), highlighting the increased rate of reductive elimination of product associated with bulky ligands with large bite angles. In many of these studies the ligands **L2** to **L6** are compared, providing useful data for our study reported here. When bound to a metal center, ligand **L4** has a smaller bite angle (84°), larger pocket angle (132°), and larger accessible molecular surface (7.578 Å^2) than those estimated for **L6** (99°, 94°, ∼4.6 Å^2). Ligand **L7** would be expected to show a similar steric profile to **L6**.[52] Consideration of these factors in concert with a likely[3] hydroacylation catalytic cycle that starts with addition of aldehyde **I** to precatalysts **16** to **19** would initially give the acyl-hydrido species **A** (Scheme 7), as observed for **1a/b**, **11**, and **15** and calculated by Morehead and Sargent for the intramolecular hydroacylation reaction of 4-pentenal by $\{Rh(\mathbf{L4})\}^+$ fragments.[22] Bifurcation of the pathway can now potentially occur: coordination of alkene results in alkene hydroacylation via intermediate **B**, while coordination of aldehyde via **D** gives aldehyde hydroacylation (the Tishchenko reaction[27]). A ligand that reveals an open metal site (e.g., **L4**, large AMS, large pocket angle, small bite angle) would allow η^2-alkene coordination (**B**). Importantly it also allows for a necessary coplanar orientation of alkene and hydride required for insertion. Aldehyde can also coordinate, but clearly alkene is preferred in this instance. With a bulkier ligand (e.g., **L7**, small AMS, small pocket angle, large bite angle) we suggest that alkene coordination is disfavored, as is the required orientation for insertion.[50] By contrast, aldehydes can coordinate η^1, which is sterically less demanding. Moreover, this more flexible coordination mode might be expected to facilitate insertion of the hydride, a process closely related to that suggested to occur in carbonyl hydrogenation by late-transition-metal hydrides (Chart 3).[53]

(45) Willis, M. C.; Randell-Sly, H. E.; Woodward, R. L.; Currie, G. S. *Org. Lett*. **2005**, *7*, 2249–2251.
(46) Tanaka, K.; Fu, G. C. *J. Am. Chem. Soc*. **2001**, *123*, 11492–11493.
(47) Casey, C. P.; Whiteker, G. T. *Isr. J. Chem*. **1990**, *30*, 299–304.
(48) van Leeuwen, P. W. N. M.; Kamer, P. C. J.; Reek, J. N. H.; Dierkes, P. *Chem. Rev*. **2000**, *100*, 2741–2770.
(49) Birkholz, M. N.; Freixa, Z.; van Leeuwen, P. *Chem. Soc. Rev*. **2009**, *38*, 1099–1118.
(50) Koide, Y.; Bott, S. G.; Barron, A. R. *Organometallics* **1996**, *15*, 2213–2226.
(51) Angermund, K.; Baumann, W.; Dinjus, E.; Fornika, R.; Gorls, H.; Kessler, M.; Kruger, C.; Leitner, W.; Lutz, F. *Chem.—Eur. J*. **1997**, *3*, 755–764.
(52) The AMS for **L7** ($Ph_2P(CH_2)_5PPh_2$) has not been reported. However those for $Ph_2P(CH_2)_4PPh_2$ and $Ph_2P(CH_2)_6PPh_2$ are both 4.66 Å^2 (ref 51), suggesting a similar AMS value for **L7**. Similarly bite angles for **L7** and pocket angles have not been reported, but might be expected to be the same as for **L6**.
(53) Clapham, S. E.; Hadzovic, A.; Morris, R. H. *Coord. Chem. Rev*. **2004**, *248*, 2201–2237.

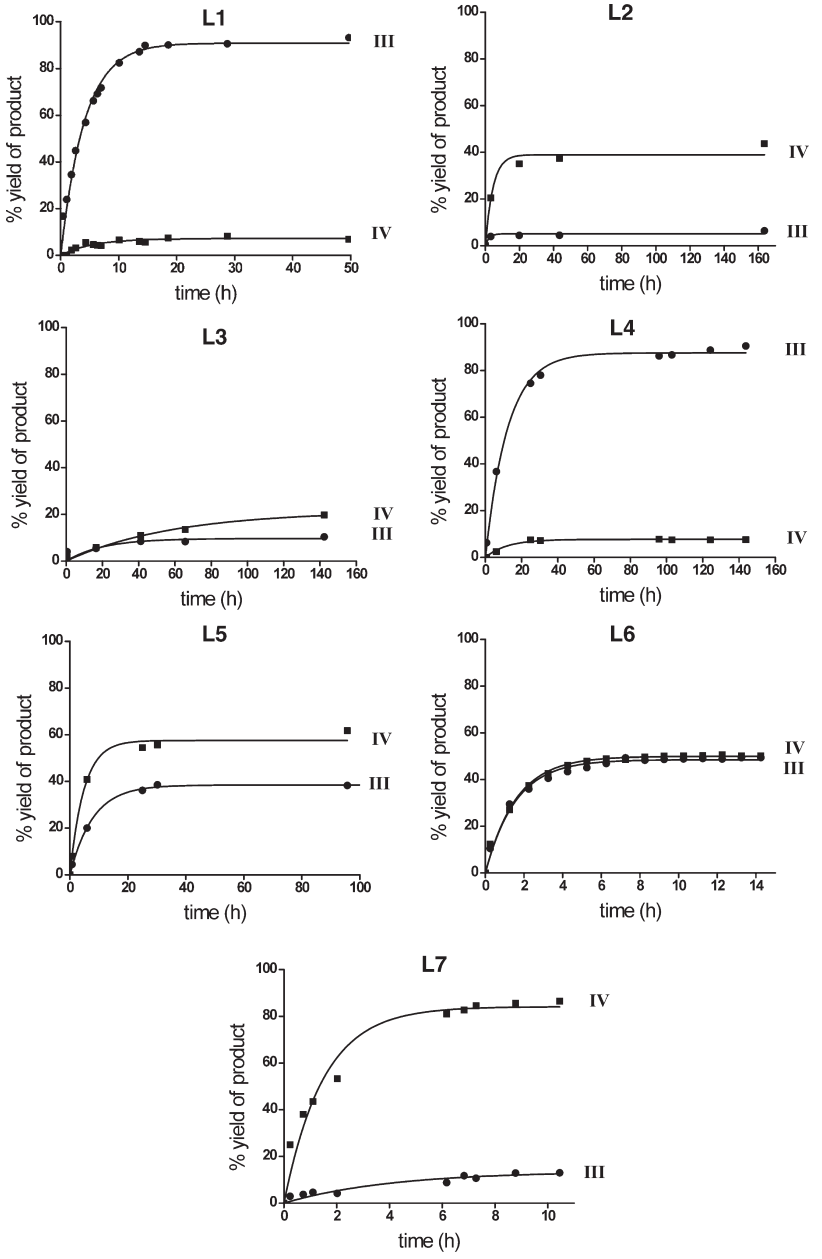

Figure 5. Relative yields of alkene hydroacylation (**III**, circles) and aldehyde hydroacylation (**IV**, squares) products using various catalyst precursors. See Table 1 for more details. Reactions carried out at room temperature, 0.043 mmol/mL of catalyst in d_6-acetone, 10 mol % catalyst loading, conversion of aldehyde **I** to **III** and **IV** products followed by ^{1}H NMR spectroscopy. Plotted lines are for comparison only.

Indeed, Dong and co-workers have recently used DFT calculations to show that a carbonyl η^1-intermediate is formed prior to hydride insertion in intramolecular ketone hydroacylation.[19] Illustrating this point further, consideration of the space-filling diagrams of the previously reported structures RhI_2(**L4**)(COMe)[54] and RhI_2(**L6**)(COMe),[55] which have an acyl group *trans* to the vacant site and are thus reasonable models for intermediate **A**, shows that the metal surface is indeed less accessible to incoming ligands for **L6** than **L4** (Figure 6). That there is an equilibrium established between **D**, **A** and **B** is shown by the effects of temperature (increased temperature favors **B**, entries 8 and 9, Table 1) and alkene concentration (increased concentrations favors **B**, entry 10, Table 1). Closely related explanations for the selectivity are that alkene binding is fast and irreversible—leading to alkene hydroacylation—for small bite angle ligands and reversible for large bite angle ligands with the reductive elimination favoring aldehyde hydroacylation. Alternatively large bite angle ligands favor reductive elimination, and thus insertion becomes rate-determining, favoring aldehyde hydroacylation. For small bite angle ligands reductive elimination is rate-determining, favoring alkene hydroacylation. Finally, the tentatively assigned CH activation product **19b** probably plays no part in the catalysis, as there is a gradual change in catalytic outcome on changing the ligand backbone length and

(54) Gonsalvi, L.; Adams, H.; Sunley, G. J.; Ditzel, E.; Haynes, A. *J. Am. Chem. Soc.* **2002**, *124*, 13597–13612.
(55) Lamb, G.; Clarke, M.; Slawin, A. M. Z.; Williams, B.; Key, L. *Dalton Trans.* **2007**, 5582–5589.

Scheme 7. Suggested Reaction Pathways for Aldehyde Hydroacylation and Alkene Hydroacylation

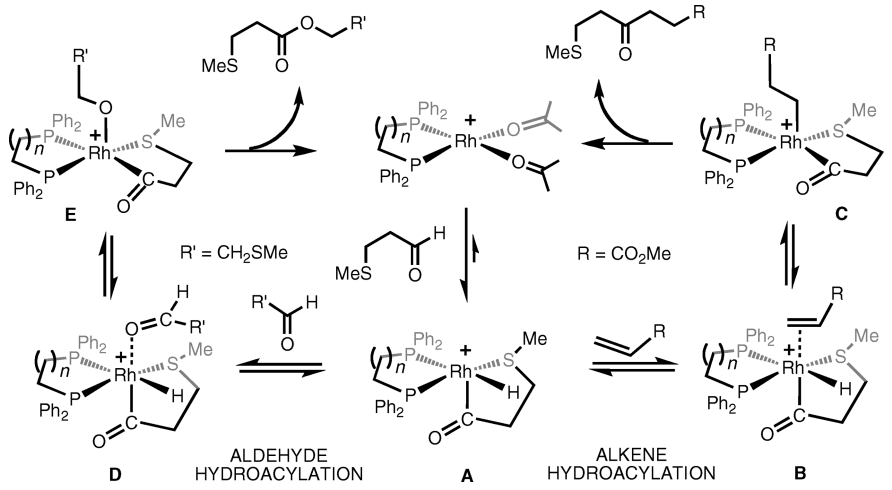

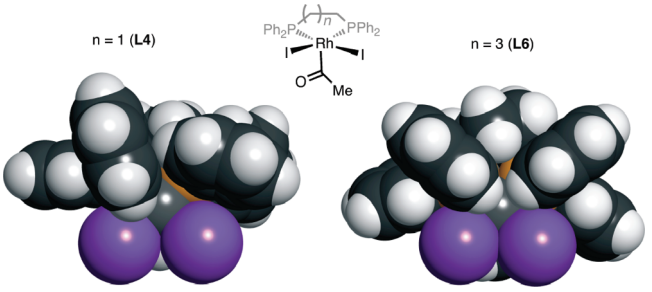

Figure 6. Space-filling diagram (van der Waals radii) of the complexes RhI_2(**L4**)(COMe)[54] and RhI_2(**L6**)(COMe)[55] showing the effect that changing the ligand backbone has on the accessible surface of the metal center (colored gray). Data were generated using the coordinates from the CCDC database (IBOZOP and HISZOZ, respectively).

Chart 3

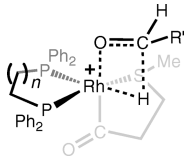

ligands **L4**−**L6** would not be expected to undergo CH activation as easily, and we see no evidence for such species by NMR spectroscopy.

Following these arguments, the DPEphos ligand, with its large bite angle of 103°,[48] might be expected to give the product of aldehyde hydroacylation, **IV**, which is not the case (entry 1). However, as previously demonstrated,[21] the DPEphos ligand can bind to the metal center in a tridentate manner (i.e., **1a**), and this extra coordination thus needs to be displaced by an incoming ligand before hydride transfer can occur (i.e., stabilizing intermediate **A**, Scheme 7). Acetone does not do this (to give an observed product), but MeCN and alkene **II** do (**B**, Scheme 7).[21] Thus we suggest that the hemilabile ligand DPEphos, **L1**, not only protects the vacant site toward decarbonylation but also appears to enforce selectivity in the reaction toward alkene hydroacylation. The large natural bite angle of DPEphos will also contribute to the rate of reductive elimination of the final product. The observation of aldehyde and alkene hydroacylation products with the POP′ and Xantphos ligands is interesting, but the low conversions and long reaction times make us reluctant to comment on the implications this has on mechanism apart from the lack of available vacant site clearly slows the rate considerably.

Conclusions

These, and previous,[13,21] results show that the overall conversion in the hydroacylation reaction can be controlled by the hemilabile nature of the chelating phosphine in the catalyst (e.g., DPEphos versus Xantphos), while the course of the reaction can also be tuned by changing the bite angle of the chelating, but not hemilabile, phosphine. These results encourage further catalyst development into controlling this atom-efficient and useful disconnection in synthesis.

Experimental Section

All manipulations, unless otherwise stated, were performed under an atmosphere of argon, using standard Schlenk-line and glovebox techniques. Glassware was oven-dried at 130 °C overnight and flamed under vacuum prior to use. CH_2Cl_2, MeCN, and pentane were dried using a Grubbs-type solvent purification system (MBraun SPS-800) and degassed by successive freeze−pump−thaw cycles.[56] 1,2-$C_6H_4F_2$ and C_6H_5F were distilled under vacuum from CaH_2 and stored over 3 Å molecular sieves. Acetone and d_6-acetone were dried over B_2O_3 and vacuum distilled twice.[57] NMR spectra were recorded on Varian Unity+ 500 MHz, Varian Mercury 300 MHz, or Bruker AVC 500 MHz spectrometers at room temperature, unless otherwise stated. Chemical shifts are quoted in ppm and coupling constants in Hz. ESI-MS were recorded on Bruker MicrOTOF and Bruker MicroOTOF-Q instruments.[58] The starting materials $\{Ph_2P(CH_2)_2\}_2O$ (POP′),[59] $Na[BAr^F{}_4]$,[60] $[Rh(nbd)Cl]_2$,[61]

(56) Pangborn, A. B.; Giardello, M. A.; Grubbs, R. H.; Rosen, R. K.; Timmers, F. J. *Organometallics* **1996**, *15*, 1518–1520.
(57) Burfield, D. R.; Smithers, R. H. *J. Org. Chem.* **2002**, *43*, 3966–3968.
(58) Lubben, A. T.; McIndoe, J. S.; Weller, A. S. *Organometallics* **2008**, *27*, 3303–3306.
(59) Thewissen, D.; Timmer, K.; Noltes, J. G.; Marsman, J. W.; Laine, R. M. *Inorg. Chim. Acta* **1985**, *97*, 143–150.
(60) Buschmann, W. E. M., J. S.; Bowman-James, K.; Miller, C. N. In *Inorganic Syntheses*; Coucouvnis, D., Ed.; Wiley-Interscience: 2002; Vol. *33*.
(61) Kranenburg, M.; van der Burgt, Y. E. M.; Kamer, P. C. J.; van Leeuwen, P. W. N. M.; Goubitz, K.; Fraanje, J. *Organometallics* **1995**, *14*, 3081–3089.

$[Rh(COD)Cl]_2$[62] and $[Rh(dppe)Cl]_2$;[63] the catalyst precursors $[Rh(nbd)(\mathbf{L5})][BAr^F_4]$,[4] $[Rh(nbd)(\mathbf{L6})][BAr^F_4]$,[4] $[Rh(nbd)(\mathbf{L7})][BAr^F_4]$,[28] [Rh(nbd)(DPEphos)][BAr^F_4],[21] and $[Rh(nbd)(POP')][BAr^F_4]$;[36] and the bis-acetone complexes $[Rh(\mathbf{L4})(acetone)_2][BAr^F_4]$,[4] $[Rh(\mathbf{L7})(acetone)_2][BAr^F_4]$,[4] $[Rh(\mathbf{L6})(acetone)_2][BAr^F_4]$,[4] and [Rh(DPEphos)$(acetone)_2$][$BAr^F_4$][21] were all prepared by published literature methods or variations thereof using $Na[BAr^F_4]$ as the chloride extracting agent. Aldehyde **I** was purchased from Aldrich and distilled before use. All other chemicals are commercial products and were used as received. Hydroacylation products **III** and **IV** were identified by comparison with previously reported data.[15] Elemental analyses for the new compounds, apart from **3**, were not satisfactorily obtained due to the fact that all crystallized with small amounts of intractable oil. NMR spectra of all the new compounds that could be isolated as solids are provided in the Supporting Information.

Crystallography. Data were acquired on a Nonius Kappa CCD diffractometer using graphite-monochromated Mo Kα radiation (λ = 0.71073 Å) and a low-temperature device;[64] data were collected using COLLECT; reduction and cell refinement were performed using DENZO/SCALEPACK.[65] Structures were solved by direct methods using DIRDIF99 (**11**)[66] or SIR2004 (**9**, **13**, **15**)[67] and refined with full-matrix least-squares on F^2 using SHELXL-97.[68] All non-hydrogen atoms were refined anisotropically. The hydride ligands (H0a and H0b in **9** and **13**, H10 in **11**, H0 in **15**) were located on the difference map and freely refined; all other hydrogen atoms were placed in calculated positions using the riding model. Disorder of the phosphine ligand in **9** was treated by modeling one of the substituents over two sites and restraining its geometry; this included using rigid body restraints. Disorder of the thioether-acyl ligand in **15** was treated by modeling part of it over two sites and restraining its geometry. Disorder of the phosphine backbone in **15** was treated by modeling the Xantphos methyl groups over two sites and restraining their geometry. Rotational disorder of the anion CF_3 groups was treated by modeling the fluorine atoms or the entire CF_3 group over two or three sites and restraining their geometry. Problematic solvent disorder in **9** and **15** was treated using the SQUEEZE algorithm.[68] Restraints to thermal parameters were applied where necessary in order to maintain sensible values. See Table S1 in the Supporting Information for further crystallographic data.

Synthesis of Complexes. [Rh(Xantphos)(nbd)][BAr^F_4], 3. Xantphos (125.5 mg, 2.17×10^{-4} mol, 2 equiv) in CH_2Cl_2 (13 mL) was added dropwise over 30 min to $[Rh(nbd)Cl]_2$ (50 mg, 1.08×10^{-4} mol, 1 equiv) in CH_2Cl_2 (1 mL). The resulting reaction mixture was then added dropwise to $Na[BAr^F_4]$ (192.2 mg, 2.17×10^{-4} mol, 2 equiv) in CH_2Cl_2 (1 mL), and the mixture was stirred for 2 h. The solution was filtered, and the filtrate was reduced to ~5 mL. Pentane was added to the filtrate until a precipitate was observed, then layered with pentane (15 mL). The solution was stored overnight at −18 °C to give orange crystals, yield = 53%, 189 mg. ^{1}H NMR (300 MHz d_6-acetone): δ 7.79 (m, 8H, BAr^F_4), 7.68 (s, 4H, BAr^F_4), 7.46−6.82 (m, 26H, Ar), 3.78 (s, 4H, nbd CH=CH), 3.52 (s, 2H, nbd CH), 1.70 (s, 6H,CH_3), 1.16 (s, 2H, nbd CH_2). ^{31}P NMR (122 MHz d_6-acetone): δ 9.74 [d, J(RhP) = 142]. ESI-MS (acetone, 60 °C, 4.5 kV) positive ion: $[M]^+$ m/z, 773.2 (M^+ calcd 773.2). Microanalysis for $C_{78}H_{52}BF_{24}OP_2Rh$ (1636.9): calcd C 57.2, H 3.20; obsd C 57.5, H 3.19.

[Rh(L)$(H)_2$(acetone)][BAr^F_4] (L = POP′, 8; Xantphos, 12). The title compounds were prepared *in situ* by placing a solution of [Rh(nbd)(L)][BAr^F_4] (6.7×10^{-6} mol) in d_6-acetone (0.3 mL) under 4 atm of hydrogen (298/77 K = 3.9). These compounds where characterized *in situ* by NMR spectroscopy and ESI-MS.

[Rh(POP′)$(H)_2$(acetone)][BAr^F_4], 8. ^{1}H NMR (500 MHz, d_6-acetone): δ 8.09−6.96 [m, 32H, Ar-H + BAr^F_4 {7.79 (8H, BAr^F_4), 7.67 (4H, BAr^F_4)}], 4.27 (br, 4H, O-CH_2), 3.18 (br, 4H, P-CH_2), −19.84 (br, fwhm = 106 Hz, 2H, Rh-H) (coordinated d_6-acetone is not observed). ^{31}P{^{1}H} NMR (202 MHz, d_6-acetone): δ 48.4 [d, J(RhP) = 121]. ^{1}H NMR (500 MHz, d_6-acetone, 225 K): δ 8.02−7.38 [m, 32H, Ar-H + BAr^F_4 {7.82 (8H, BAr^F_4), 7.73 (4H, BAr^F_4)}], 4.35 (m, 2H, O-CH_2), 4.16 (m, 2H, O-CH_2′), 3.42 (m, 2H, P-CH_2), 2.94 (m, 2H, P-CH_2′), −19.25 [dtd, J(RhH) = 24.5, J(PH) = 13.9, J(HH) = 10.7, 1H, Rh-H], −20.27 [dtd, J(RhH) = 24.3, J(PH) = 13.4, J(HH) = 10.7, 1H, Rh-H]. ^{31}P{^{1}H} NMR (202 MHz, d_6-acetone, 225 K): δ 49.0 [d, J(RhP) = 121]. ESI-MS (acetone, 60 °C, 4.5 kV) positive ion: (minor peak) $[M]^+$ m/z = 605.1 (calcd 605.1); (major peak) [M − acetone]$^+$ m/z = 547.1 (calcd 547.1). ESI-MS (acetone, 60 °C, 4.5 kV) positive ion: m/z, 773.2 (M^+ calcd 773.2).

[Rh(Xantphos)$(H)_2$(acetone)][BAr^F_4], 12. ^{1}H NMR (500 MHz, d_6-acetone): δ 8.34−6.85 [m, 38H, Ar-H + BAr^F_4 {7.79 (8H, BAr^F_4), 7.68 (4H, BAr^F_4)}], 2.25−1.54 (br m, 6H, CH_3), −18.81 (1 H, br, Rh-H), −19.00 (br, 1H, Rh-H). ^{31}P{^{1}H} NMR (202 MHz, d_6-acetone): δ 45.4 [d, J(RhP) = 121]. ^{1}H NMR (500 MHz, d_6-acetone, 225 K): δ 8.26−7.20 [m, 38H, Ar-H + BAr^F_4 {7.83 (8H, BAr^F_4), 7.73 (4H, BAr^F_4)}], 1.94 (s, 3H, CH_3), 1.70 (s, 3H, CH_3′), −18.44 [dtd, J(RhH) = 22.1, J(PH) = 12.8, J(HH) = 9.5, 1H, Rh-H], −19.17 [dtd, J(RhH) = 31.4, J(PH) = 14.5, J(HH) = 9.2, 1H, Rh-H]. ^{31}P{^{1}H} NMR (202 MHz, d_6-acetone, 225 K): δ 46.0 [d, J(RhP) = 121]. ESI-MS (acetone, 60 °C, 4.5 kV) positive ion: (minor peak) $[M]^+$ m/z = 741.15 (calcd 741.15); (major peak) [M − acetone]$^+$ m/z = 683.11 (calcd 683.10).

[Rh(L)$(H)_2$(NCMe)][BAr^F_4] (L = POP′, 9, Xantphos, 13). [Rh(L)(nbd)][BAr^F_4] (1.5×10^{-2} mmol) in d_6-acetone (0.3 mL) was freeze−thaw−degassed and backfilled with hydrogen at 77 K. The solution was shaken for 30 min at room temperature. The solution was then freeze−thaw−degassed again and backfilled with argon at room temperature. Acetonitrile (7.8 μL, 1.5×10^{-1} mmol, 10 equiv) was added and the solution shaken for 30 min. The solution was transferred into a Young's crystallization tube. Solvent was removed *in vacuo* and the resulting residue washed with pentane (3 × 2 mL), then recrystallized by diffusion of hexane into a fluorobenzene solution of the crude product to yield colorless crystals. Yield: 43%, 9.3 mg and 73%, 17.4 mg, respectively.

[Rh(POP′)$(H)_2$(NCMe)][BAr^F_4], 9. ^{1}H NMR (500 MHz, CD_2Cl_2): δ 7.85−7.30 [m, 32 H, Ar-H + BAr^F_4 {7.72 (8H, BAr^F_4), 7.56 (4H, BAr^F_4)}], 4.10 (m, 2H, O-CH_2), 3.53 (m, 2H, O-CH_2′), 2.92 (m, 4H, P-CH_2), −16.69 [dtd, J(RhH) = 21.3, J(PH) = 12.3, J(HH) = 8.9, 1H, Rh-H], −19.39 [dtd, J(RhH) = 21.9, J(PH) = 13.1, J(HH) = 8.8, 1H, Rh-H]. ^{31}P{^{1}H} NMR (202 MHz, CD_2Cl_2): δ 47.1 [d, J(RhP) = 120 Hz]. ESI-MS (fluorobenzene, 60 °C, 4.5 kV) positive ion: (minor peak) $[M]^+$ m/z = 588.0922 (calcd 588.1087); (major peak) [M − MeCN]$^+$ m/z = 547.0705 (calcd 547.0821).

[Rh(Xantphos)$(H)_2$(NCMe)][BAr^F_4], 13. ^{1}H NMR (500 MHz, CD_2Cl_2): δ 7.92−7.29 [m, 38H, Ar-H + BAr^F_4 {7.72 (8H, BAr^F_4), 7.55 (4H, BAr^F_4)}], 1.91 (s, 3H, CH_3), 1.51 (s, 3H, CH_3′), 1.16 (s, 3H, coordinated MeCN CH_3), −15.36 [dtd, J(RhH) = 20.3, J(PH) = 12.3, J(HH) = 7.8, 1H, Rh-H], −19.36 [dtd, J(RhH) = 30.8, J(PH) = 13.9, J(HH) = 7.8, 1H, Rh-H]. ^{31}P{^{1}H} NMR (202 MHz, CD_2Cl_2): δ 44.8 [d, J(RhP) = 117 Hz]. ESI-MS (fluorobenzene, 60 °C, 4.5 kV) positive ion: (minor peak) $[M]^+$ m/z = 724.0896 (calcd 724.1400); (major peak) [M − MeCN]$^+$ m/z = 683.0745 (calcd 683.1134).

(62) Giordano, G.; Crabtree, R. H. *Inorg. Synth.* **1990**, *28*, 88.
(63) Uehara, A.; Bailar, J. C. *J. Organomet. Chem.* **1982**, *239*, 11–15.
(64) Cosier, J.; Glazer, A. M. *J. Appl. Crystallogr.* **1986**, *19*, 105–107.
(65) Otwinowski, Z.; Minor, W. In *Macromolecular Crystallography, Part A*; Carter, C. W., Sweat, R. M., Eds.; Academic Press: New York, 1997; Vol. *276*.
(66) Beurskens, P. T.; Beurskens, G.; de Gelder, R.; Garcia-Granda, S.; Gould, R. O.; Israel, R.; Smits, J. M. M. *The DIRDIF-99 program system*; University of Nijmegen: Netherlands, 1999.
(67) Burla, M. C.; Caliandro, R.; Camalli, M.; Carrozzini, B.; Cascarano, G. L.; De Caro, L.; Giacovazzo, C.; Polidori, G.; Spagna, R. *J. Appl. Crystallogr.* **2005**, *38*, 381–388.
(68) Spek, A. L. *J. Appl. Crystallogr.* **2003**, *36*, 7–13.

[Rh(L)(η^2-H_2C=CHCOOMe))][BAr^F_4] (L = POP′, 10; Xantphos, 14). The title compounds were prepared *in situ* by placing a solution of [Rh(L)nbd][BAr^F_4] (6.7×10^{-3} mmol) in d_6-acetone (0.3 mL) under 4 atm of hydrogen, followed by addition of methyl acrylate (1.2 mL, 1.3×10^{-2} mmol, 2 equiv) under an atmosphere of argon. These compounds where characterized *in situ* by NMR spectroscopy and ESI-MS.

[Rh(POP′)(η^2-H_2C=CHCOOMe)][BAr^F_4], 10. ^{1}H NMR (500 MHz, d_6-acetone): δ 8.11−7.34 (m, 32H, Ar-H + BAr^F_4 {7.79 (8H, BAr^F_4), 7.68 (4H, BAr^F_4)}), 4.41 (m, 2H, O-CH_2), 4.31 (m, 2H, O-CH_2′), 3.60 (br m, 1H H_2C=CH), 3.38 (s, 3H, OMe), 3.05 (m, 2H, P-CH_2), 2.90 (br m, 2 + 1 H, P-CH_2′ + H_2C=CH), 2.64 (m, 1H, H_2C=CH). Also observed: 6.41−5.82 (br m, free acrylate, H_2C=CH), 3.70 (br s, free acrylate OMe). $^{31}P\{^1H\}$ NMR (202 MHz, d_6-acetone): δ 39.1 [d, J(RhP) = 129 Hz]. ESI-MS (acetone, 60 °C, 4.5 kV) positive ion: $[M]^+$ m/z, 631.1 (calcd 631.1). ESI-MSMS (631.1): m/z = 545.1 (M^+ − $CH_2CHCO_2CH_3$ calcd 545.1).

[Rh(Xantphos)(η^2-H_2C=CHCOOMe)][BAr^F_4], 14. ^{1}H NMR (500 MHz, d_6-acetone): δ 8.20−7.12 [m, 38H, Ar-H + BAr^F_4 {7.79 (8H, BAr^F_4), 7.68 (4H, BAr^F_4)}], 3.53 (s, 3H, OMe), 3.38 (m, 1H, H_2C=CH), 2.67 (m, 1H, H_2C=CH), 2.17 (m, 1H, H_2C=CH, coincident with a norbornane peak), 1.90 (s, 6H, CH_3). Also observed: 6.40−5.76 (br m, free acrylate, H_2C=CH), 3.70 (br s, free acrylate OMe). $^{31}P\{^1H\}$ NMR (202 MHz, d_6-acetone): δ 34.23 [br s, fwhm = 1187 Hz]. ESI-MS (C_6H_5F, 60 °C, 4.5 kV) positive ion: $[M]^+$ m/z, 767.1 (calcd 767.1).

[Rh(L)(MeSCH_2CH_2CO)(H)][BAr^F_4] (L = POP′, 11; Xantphos, 15). [Rh(L)(nbd)][BAr^F_4] (6.1×10^{-2} mmol) in acetone (3 mL) was freeze−thaw−degassed and backfilled with hydrogen at 77 K. The solution was stirred for 1 h at room temperature. The solution was then freeze−thaw−degassed again and backfilled with argon at room temperature. Methyl acrylate (8.2 μL, 9.2×10^{-2} mmol, 1.5 equiv) was added and the solution stirred for 4 h, after which 3-(methylthio)propionaldehyde (9.1 μL, 9.2×10^{-2} mmol, 1.5 equiv) was added and the solution stirred for a further hour. The solvent was removed *in vacuo* and the resulting residue washed with pentane (2 × 3 mL), then recrystallized by diffusion of pentane into a fluorobenzene solution of the crude product to yield colorless crystals. Yield: 63%, 69.4 mg and 35%, 31.8 mg, respectively.

[Rh(POP′)(MeSCH_2CH_2CO)(H)][BAr^F_4], 11. ^{1}H NMR (400 MHz CD_2Cl_2): δ 8.23−7.30 [m, 32 H, Ar-H + BAr^F_4 {7.72 (8H, BAr^F_4), 7.61 (4H, BAr^F_4)}], 4.01 (m, 2H, CH_2), 3.05−2.79 (m, 6H, CH_2), 2.37 (br m, 2H, CH_2), 1.79 [d, J(HH) 1.8 Hz, 3H, SCH_3], 1.67 (br m, 2H, CH_2), −9.58 [br d, J(RhH) 24 Hz, 1H, RhH]. ^{1}H−^{1}H COSY NMR (400 MHz, CD_2Cl_2): Correlation observed between SCH_3 and hydride. $^{31}P\{^1H\}$ NMR (162 MHz, CD_2Cl_2): δ 31.1 (br s, fwhm = 513 Hz). $^{31}P\{^1H\}$ NMR (202 MHz, d_6-acetone, 225 K): ABX coupling pattern observed: δ 34.6 [dd, J(PP) = 309 Hz, J(RhP) = 128 Hz], 28.5 [dd, J(PP) = 309 Hz, J(RhP) = 133 Hz]. ESI-MS (acetone, 60 °C, 4.5 kV) positive ion: $[M]^+$ m/z = 649.1022 (calcd 649.0961).

[Rh(Xantphos)(MeSCH_2CH_2CO)(H)][BAr^F_4], 15. ^{1}H NMR (500 MHz, d_6-acetone): δ 8.48−7.36 [m, 38H, Ar-H + BAr^F_4 {7.79 (8H, BAr^F_4), 7.68 (4H, BAr^F_4)}], 2.62 (br s, fwhm = 77 Hz, 2H, CH_2), 2.04 (br, 2H, CH_2, coincident with CD_2HCOCD_3 peak), 1.97 (s, 3H, CH_3), 1.51 (s, 3H, CH_3′), 1.47 [d, J(HH) = 1.8 Hz, 3H, SCH_3], −8.72 [br d, J(RhH) = 23 Hz, 1H, Rh-H]. $^{31}P\{^1H\}$ NMR (202 MHz, d_6-acetone): δ 32.8 (br s, fwhm = 478 Hz). ^{1}H−^{1}H COSY NMR (500 MHz, d_6-acetone): Correlation observed between SCH_3 and hydride. ^{1}H NMR (500 MHz, d_6-acetone, 240 K): δ 8.58−7.24 [m, 38H, Ar-H + BAr^F_4 {7.81 (8H, BAr^F_4), 7.72 (4H, BAr^F_4)}], 2.80 (m, 1H, CH_2), 2.37 (m, 1H, CH_2), 2.10 (m, 1H, CH_2), 1.94 (s, 3H, CH_3), 1.82 (m, 1H, CH_2) 1.47 (s, 3H, CH_3′), 1.38 (s, 3H, SCH_3), −8.65 [br dd, J(RhH) = 23 Hz, J(PH) = 7 Hz, 1H, Rh-H]. $^{31}P\{^1H\}$ NMR (202 MHz, d_6-acetone, 257 K): ABX coupling pattern observed: δ 35.22 (dd, J(PP) = 300, J(RhP) = 124), 32.04 [dd, J(PP) = 300, J(RhP) = 127]. ESI-MS (acetone, 60 °C, 4.5 kV) positive ion: $[M]^+$ m/z = 785.1221 (calcd 785.1274).

[Rh(nbd)(L4)][BAr^F_4], 16 (improved synthetic route). [Rh(dppe)Cl]$_2$ (50 mg, 4.9×10^{-2} mmol) and Na[BAr^F_4] (86.8 mg, 9.8×10^{-2} mmol, 2 equiv) were stirred together in $C_6H_4F_2$ (10 mL) for 20 min. C_7H_8 (norbornadiene) (24.9 μ, 2.5×10^{-1} mmol, 5 equiv) was added to the mixture and the mixture stirred for 2 h. The mixture was filtered and pentane (25 mL) added to the filtrate. The solution was stored overnight at −18 °C. The solution was reduced to 10 mL and filtered, and hexane (25 mL) was added to the filtrate. The solvent was removed *in vacuo*, leaving an orange powder. Yield: 45%, 65 mg. ^{1}H NMR (300 MHz, d_6-acetone): δ 7.50−7.88 (m, 32H, BAr^F_4 and Ph), 5.51 (m, 4H, nbd CH=CH), 4.26 (m, 2H, nbd CH), 2.58 (m, 4H, PCH_2), 1.82 (s, 2H, nbd CH_2). ^{31}P NMR (122 MHz, d_6-acetone): δ 55.9 [d, J(RhP) = 157].

[Rh(L7)(acetone)$_2$][BAr^F_4], 19a, [Rh(PPh$_2$CH$_2$CH$_2$CHCH$_2$CH$_2$PPh$_2$)(H)(acetone)$_2$][BAr^F_4], 19b*, and [Rh(L7)(H)$_2$(acetone)$_2$][BAr^F_4], 19c$^\$$. The title compounds were prepared *in situ* by placing a solution of [Rh(nbd)(**L7**)][BAr^F_4] (6.7×10^{-6} mol) in d_6-acetone (0.3 mL) under 4 atm of hydrogen. These compounds where characterized *in situ* by NMR spectroscopy and ESI-MS. ^{1}H NMR (500 MHz, d_6-acetone): δ 7.91−7.31 [m, 32H, Ar-H + BAr^F_4 {7.80 (8H, BAr^F_4), 7.68 (4H, BAr^F_4)}], 2.92 (m, 2H, PCH_2CH_2), 2.47 (m, 4H, $PCH_2CH_2CH_2$), 1.86 (m, 4H, PCH_2), −21.68 [dt, J(RhH) = 27, J(PH) = 16, Rh-H]*, −22.30 [dt, J(RhH) = 35, J(PH) = 11, Rh-H]$^\$$ (coordinated d_6-acetone is not observed). $^{31}P\{^1H\}$ NMR (202 MHz, d_6-acetone): δ 55.3 [d, relative 0.8 P, J(RhP) = 133]$^\$$, 37.3 [d, relative 10P, J(RhP) = 201], 35.8 [d, relative 2P, J(RhP) = 115]*. *Denotes selected signals due to **19b**. $^\$$Denotes selected signals due to **19c**. ESI-MS (acetone, 60 °C, 4.5 kV) positive ion: (minor peak) $[M]^+$ m/z = 659.2 (calcd 659.2); (major peak) [M − acetone]$^+$ m/z = 601.1 (calcd 601.1); (major peak) [M − (acetone)$_2$]$^+$ m/z = 543.1 (calcd 543.1).

General Method for Catalysis. In a typical experiment [Rh(**L**)(nbd)][BAr^F_4] (1.5×10^{-2} mmol) was placed into a New Era high-pressure NMR sample tube. d_6-Acetone (0.3 mL) was added by cannula and the solution placed under an H_2 atmosphere for 5 min to generate the active catalyst. Under an argon atmosphere **I** (15 mL, 1.5×10^{-1} mmol, 10 equiv) and **II** (13.5 mL, 1.5×10^{-1} mmol, 10 equiv) were added by syringe. The solution was kept at ambient temperature (22 °C) and the reaction followed *in situ* by ^{1}H NMR spectroscopy. Compounds **III** and **IV** were identified by comparison with published data.[15]

Acknowledgment. We thank the EPSRC, the University of Oxford, and the John Fell Fund (University of Oxford) for support and the referees for insightful comments.

Supporting Information Available: Simulated and experimental NMR spectra for **8** and **12**; experimental NMR spectra for **9**, **11**, **13**, and **15**; and crystallographic collection and refinement parameters for **9**, **11**, **13**, and **15**. This material is available free of charge via the Internet at http://pubs.acs.org.